Determination of Monomer Conformations in Noncrystalline Solid Polymers by Two-Dimensional NMR Exchange Spectroscopy

Gary Dabbagh, David P. Weliky,† and Robert Tycko*

AT&T Bell Laboratories, 600 Mountain Avenue, Murray Hill, New Jersey 07974

Received February 2, 1994; Revised Manuscript Received April 21, 1994®

ABSTRACT: We propose and demonstrate a new approach to the determination of the conformations of molecules or monomers in noncrystalline solids. The method makes use of two-dimensional NMR exchange spectroscopy in combination with specific isotopic labeling. We present experimental results on specifically labeled poly(methyl methacrylate), poly(methyl acrylate), and poly(ethyl methacrylate). Through comparisons between the experimental and simulated two-dimensional spectra, we determine that the ester side groups of poly(methyl methacrylate) and poly(methyl acrylate) have planar, trans conformations and that the side groups of poly(ethyl methacrylate) are also predominantly in the planar, trans conformation in the noncrystalline solid state. We discuss potential applications of this approach in structural studies of synthetic polymers, biological systems, and other disordered solids.

I. Introduction

The determination of molecular conformations in noncrystalline solids is an important problem with ramifications in polymer science, physical chemistry, and structural biochemistry. While various techniques for addressing this problem exist, including diffraction techniques, infrared spectroscopy, and magnetic resonance techniques, none have general applicability in complex systems and none provide complete conformational information. In this paper, we demonstrate a new approach to the determination of molecular conformations in noncrystalline solids, based on two-dimensional nuclear magnetic resonance (NMR) exchange spectroscopy.[1] Although this approach is also not entirely general, since it depends on the ability to specifically isotopically label the interesting region of the system, it has the potential of providing quite detailed conformational information about (at least) specific components of systems of arbitrary size and complexity. The information provided by the techniques described in this paper may not be accessible by any other current experimental technique.

The systems studied in this work are the familiar noncrystalline polymers poly(methyl methacrylate), poly(methyl acrylate), and poly(ethyl methacrylate). These polymers were chosen for our initial studies because of their widespread importance and because they comprise a series that could be specifically ^{13}C-labeled with relative ease. We focus on a specific aspect of the monomer conformations in the polymers, namely, the conformation of the ester side groups, shown in Figure 1. In the notation of Figure 1, the angles Θ_1, Θ_2, and Θ_3 are determined by chemical bonding considerations. The dihedral angles χ_1 and χ_2 may vary in principle. It is these angles, in the noncrystalline solid state, that we attempt to determine from our two-dimensional NMR exchange experiments. We adopt a convention in which the all-trans, planar conformation corresponds to $\chi_1 = \chi_2 = 0°$.

The use of two-dimensional NMR exchange spectroscopy as a probe of molecular conformations in solids relies on the fact that the NMR frequencies of nuclei associated with particular chemical functional groups or chemical bonds depend on the orientation of these functional groups

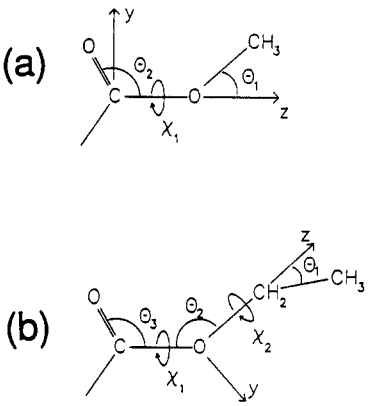

Figure 1. Ester side groups of poly(methyl methacrylate) and poly(methyl acrylate) (a) and of poly(ethyl acrylate) (b). The conformations of these groups are defined by the dihedral angles χ_1 and χ_2. Two-dimensional ^{13}C NMR exchange spectroscopy is used to determine the values of these angles.

or bonds relative to the external magnetic field in the NMR experiment.[2] A measurement of the NMR frequencies of nuclei associated with a *single* functional group or bond in a noncrystalline solid (i.e., of a one-dimensional NMR line shape) therefore provides information about the orientational probability distribution of that single functional group or bond. A measurement of the correlations between the NMR frequencies of nuclei associated with *two different* functional groups or bonds in a single molecule or monomer provides information about the correlations between the orientations of the two functional groups or bonds. The orientational correlations specify the conformation of the molecule or monomer.

In a two-dimensional NMR exchange experiment, one effectively measures the initial NMR frequencies of nuclear magnetization at a particular site (in the t_1 dimension), waits an exchange period τ, and then measures the final NMR frequencies of the same magnetization (in the t_2 dimension). Several mechanisms can produce a difference between the initial and final frequencies. In the experiments described below, the only important mechanism is the exchange of magnetization (also called spin diffusion) between isotopically labeled sites, driven by nuclear magnetic dipole–dipole couplings.[3-5] It is the magnetization exchange process that permits the correlations between NMR frequencies of nuclei associated with different functional groups or bonds to be measured.

* Author to whom correspondence should be addressed.
† Current address: Department of Chemistry, University of Chicago, Chicago, IL 60637.
® Abstract published in *Advance ACS Abstracts*, August 15, 1994.

0024-9297/94/2227-6183$04.50/0

Two-dimensionl NMR exchange spectroscopy has already been exploited extensively in studies of molecular orientational dynamics in solids.[6,7] In these *dynamical studies*, the dominant mechanism that produces differences between initial and final NMR frequencies is molecular reorientation, not magnetization exchange. Applications of two-dimensional NMR exchange spectroscopy in *structural studies*, by us[8-10] and by others,[11-13] have so far addressed questions related to the packing of molecules in polycrystalline and noncrystalline solids rather than the molecular conformations. Of course, two-dimensional NMR exchange spectroscopy is also a very well established technique for studying chemical exchange processes and molecular structures *in liquids*, where the spectra, the interactions, and the mechanisms are quite different from those discussed in this paper.[14-16]

Two variants of the two-dimensional exchange technique are used in the experiments. We call the first variant, which we apply to poly(methyl methacrylate) and poly(methyl acrylate), two-dimensional CSA/CSA NMR exchange spectroscopy. In the CSA/CSA exchange experiments, the NMR frequencies are determined by anisotropic chemical shift (CSA) interactions in both dimensions. This variant is applicable to molecules or monomers that are singly-labeled at two sites, specifically the carboxyl carbon and the methoxy carbon of the ester side group in our experiments. We call the second variant, which we apply to poly(ethyl methacrylate), two-dimensional DD/CSA NMR exchange spectroscopy.[10] In the DD/CSA exchange experiments, the NMR frequencies are determined by magnetic dipole–dipole interactions in one dimension and by the CSA in the other dimension. This variant is applicable to molecules or monomers that are doubly-labeled on one bond and singly-labeled at one functional group, specifically the ethoxy carbon–carbon bond and the carboxyl carbon of the ester side group.

In section II, we describe the synthesis and characterization of the labeled polymers and the implementation of the two-dimensional NMR exchange techniques. In sections III and IV, we present the experimental results and the analysis of these results by comparison with simulated two-dimensional spectra. In section V, we discuss the significance of the results and point out several promising areas for future applications of the two-dimensional NMR exchange techniques in structural studies.

II. Materials and Methods

A. Synthesis and Characterization of ^{13}C-Labeled Polymers. The 2D NMR experiments described below depend on the synthesis of polymers from mixtures of ^{13}C-labeled and unlabeled monomers. In the case of poly(methyl methacrylate) (PMMA) and poly(methyl acrylate) (PMA), the labeled monomers are ^{13}C-enriched at both the carboxyl and the methoxy sites. In the case of poly(ethyl methacrylate) (PEMA), the labeled monomers are ^{13}C-enriched at the carboxyl and at both ethoxy sites. Dilution of the labeled monomers in unlabeled monomers suppresses carbon–carbon couplings between different monomers. This allows the 2D ^{13}C NMR spectra to reflect primarily the carbon–carbon couplings within individual monomers and therefore to probe primarily the conformations of individual monomers rather than the overall polymer chain conformation or chain packing.

[$^{13}C_2$]Methyl methacrylate was synthesized as follows. First, (2-propenyl)magnesium bromide was prepared by addition of 2-bromopropene (Aldrich) to magnesium in THF at 75 °C. This was converted to [^{13}C]methacrylic acid in 53% yield by reaction with $^{13}CO_2$ (99% enriched, Cambridge Isotopes Laboratories), acidification with 20% HCl, ether extraction, extraction with $NaOH_{(aq)}$, reacidification, and a second ether extraction. After drying with Na_2SO_4 and evaporation of the ether, [^{13}C]methacrylic acid was converted to [^{13}C]sodium methacrylate by addition to 1 equiv of NaOH in methanol, followed by drying. This was converted to [$^{13}C_2$]methyl methacrylate in 44% yield by reaction with 1.3 equiv of [^{13}C]iodomethane (99% enriched, Aldrich) in DMSO, precipitation of NaI with ether, removal of DMSO with a brine extraction, drying with Na_2SO_4, and evaporation of the ether. To form the partially labeled polymer, [$^{13}C_2$]methyl methacrylate was diluted in unlabeled methyl methacrylate (Aldrich), passed through a basic alumina column to remove polymerization inhibitors, dissolved in THF, and deoxygenated by repeated freeze–pump–thaw cycles. Polymerization was initiated with benzoyl peroxide and proceeded for 22 h at 80 °C. PMMA was precipitated with methanol, filtered, and dried.

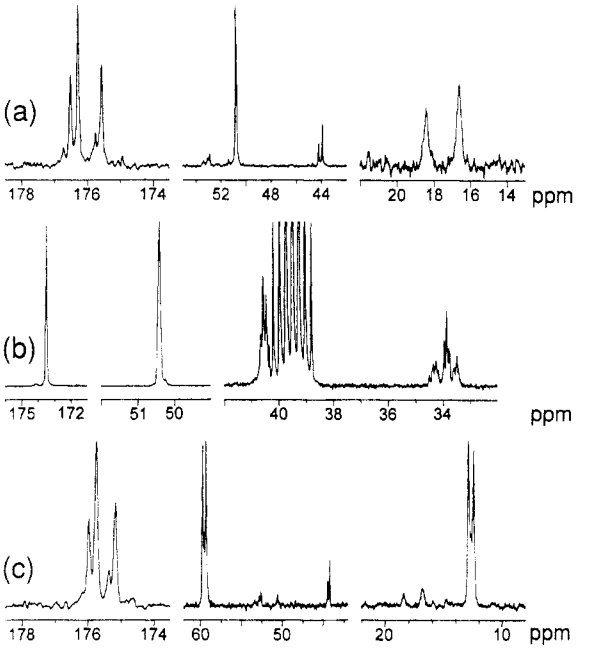

Figure 2. High-resolution ^{13}C NMR spectra at 90 MHz of selectively ^{13}C-enriched PMMA (a), PMA (b), and PEMA (c) in DMSO-d_6, recorded at 100, 100, and 130 °C, respectively. Frequency scales are relative to TMS.

[$^{13}C_2$]Methyl acrylate was synthesized as follows. First, [^{13}C]-acrylic acid was prepared by addition of 27 mmol of vinylmagnesium bromide (1.0 M in THF, Aldrich) to 1 L of $^{13}CO_2$ with 50 mL of THF at −78 °C, followed by warming for reaction at room temperature for 30 min and quenching with 1 N HCl. The acrylic acid was extracted with ether, dried with Na_2SO_4, filtered, and concentrated by evaporation of the ether. [^{13}C]Diazomethane in ether was prepared from [^{13}C]-*N*-methyl-*N*-nitroso-*p*-toluenesulfonamide. Reaction of [^{13}C]acrylic acid with [^{13}C]-diazomethane produced the desired [$^{13}C_2$]methyl acrylate. After dilution with unlabeled methyl acrylate (Aldrich), polymerization to PMA proceeded as for PMMA.

[$^{13}C_3$]Ethyl methacrylate was synthesized in 55% yield by the addition of 1.0 equiv of [$^{13}C_2$]iodoethane (98% enriched, Aldrich) to [^{13}C]sodium methacrylate in DMSO at room temperature. After low-pressure distillation away from NaI, unlabeled ethyl methacrylate (Aldrich) was added to produce the desired level of enrichment, and the ethyl methacrylate was distilled away from the DMSO. After removal of inhibitors and deoxygenation, polymerization was initiated with benzoyl peroxide (4.0 mg added to 0.9 g of ethyl methacrylate) and proceeded for 20 h at 80 °C. PEMA was precipitated with petroleum ether, filtered, and dried.

The PMMA, PMA, and PEMA samples had glass transition temperatures (T_g) of 121, 9, and 76 °C, respectively, as determined by differential scanning calorimetry. High-resolution ^1H and ^{13}C NMR spectra at elevated temperatures in perdeuterated dimethyl sulfoxide (DMSO-d_6) solution confirmed the chemical structures and purity of the polymers. These spectra were entirely consistent with previously published spectra of high molecular weight polymers generated by free-radical polymerization.[17,18] The high-resolution ^{13}C NMR spectra are shown in Figure 2. For

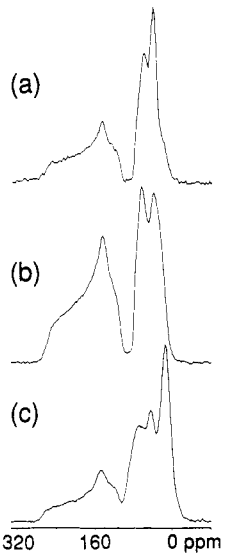

Figure 3. One-dimensional solid-state ^{13}C NMR spectra at 100.47 MHz of selectively ^{13}C-enriched PMMA (a), PMA (b), and PEMA (c), recorded at +23, −100, and −100 °C, respectively.

PMMA (Figure 2a) and PEMA (Figure 2c), the intensity distributions of the carboxyl resonances (174–178 ppm), methyl resonances (16–20 ppm), and methine resonances (43–45 ppm) indicate that the ratio of meso–racemic (mr) to racemic–racemic (rr) triads is roughly 0.61 ± 0.05. These polymers are therefore predominantly syndiotactic, as expected for free-radical polymerization, with a roughly 74% probability of racemic addition. For PMA (Figure 2b), the methylene ^{13}C NMR resonances (centered around 34 ppm) and the methylene ^{1}H NMR resonances (not shown) indicate an essentially atactic microstructure, with roughly equal numbers of meso and racemic diads. From the relative intensities of the ^{13}C-enriched and natural-abundance peaks in Figure 2, we determine that 2.2, 7.3, and 4.5% of the monomers are (multiply) ^{13}C-labeled in the PMMA, PMA, and PEMA samples, respectively.

One-dimensional solid-state ^{13}C NMR spectra of the three polymer samples, obtained at 100.47 MHz with standard cross-polarization and proton decoupling methods, are shown in Figure 3. These spectra show the chemical shift anisotropy (CSA) powder pattern line shapes that are typical of noncrystalline, unoriented organic solids. In all cases, the carboxyl carbons give rise to a CSA powder pattern (100–280 ppm) that is resolved from the signals of the other carbons (−25 to +100 ppm). This fact greatly simplifies the appearance and analysis of the two-dimensional spectra discussed below. From the spectra in Figure 3, we determine the principal values (δ_{11}, δ_{22}, δ_{33}) of the carboxyl CSA tensors to be (266, 148, 108), (259, 143, 108), and (264, 148, 109) for PMMA, PMA, and PEMA, respectively (in ppm relative to TMS). We determine the principal values of the methoxy CSA tensors to be (79, 62, 13) for both PMMA and PMA. These values are in good agreement with a previous solid-state NMR study of PMMA.[19] Magnetic dipole–dipole couplings between the ^{13}C labels affect the line shapes in Figure 3. For the ethoxy resonances in PEMA, this effect is substantial because the dipole–dipole coupling between the two ethoxy carbons (maximum splitting ≈ 6 kHz) has the same magnitude as the CSA. For the carboxyl resonances of all three polymers and for the methoxy resonances of PMMA and PMA, this effect is a minor one, leading to a small broadening (<1 kHz) of the CSA powder patterns.

B. Two-Dimensional NMR Exchange Spectroscopy. Figure 4 shows the radio-frequency (rf) pulse sequences used to obtain the two-dimensional NMR spectra discussed below. These sequences have been described in detail previously.[1,8,10] CSA/CSA exchange spectra, i.e., two-dimensional spectra in which the NMR frequencies in both dimensions are determined primarily by the CSA tensors, are obtained with the sequence in Figure 4a; DD/CSA exchange spectra, i.e., two-dimensional spectra in which the NMR frequencies in the ν_1 dimension are determined primarily by homonuclear dipole–dipole couplings and those in the ν_2 dimension are determined primarily by the

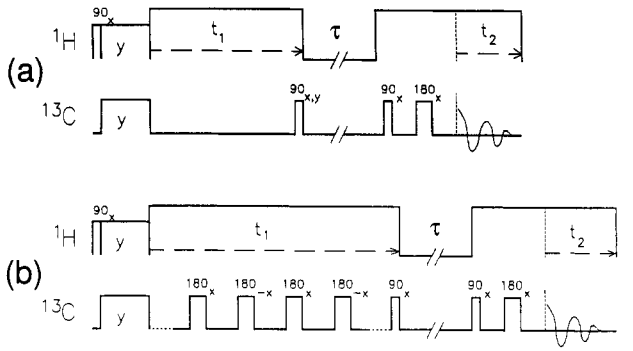

Figure 4. Rf pulse sequences used to obtain two-dimensional ^{13}C NMR exchange spectra: (a) sequence for CSA/CSA exchange experiments; (b) sequence for DD/CSA exchange experiments.

CSA tensors, are obtained with the sequence in Figure 4b. The standard double-resonance techniques of cross-polarization and proton decoupling are used in both sequences. The most significant difference between them is the application of a Carr–Purcell train of π pulses during the t_1 period in Figure 4b. In the ideal case, and to a good approximation in the actual experiments, the Carr–Purcell train averages out the chemical shifts and CSA in t_1, leaving the homonuclear dipole–dipole couplings as the only significant interactions in t_1.[20] In the DD/CSA exchange experiments, the t_1 period is incremented in 100 μs steps, with two π pulses per increment. In the CSA/CSA exchange experiments, the t_1 period is incremented in 15 μs steps. The dwell time (digitization interval in t_2) is 15 μs in both types of exchange experiments. In both sequences in Figure 4, digitization of the NMR signals in t_2 begins after a $\pi/2$–π Hahn echo sequence. The Hahn echo proved to be necessary for the attainment of undistorted powder pattern line shapes and flat baselines in the two-dimensional spectra.

Imperfect π pulses in the Carr–Purcell train in Figure 4b can lead to enhanced signal at $\nu_1 = 0$ at the expense of signals at $\nu_1 \neq 0$ in the DD/CSA exchange spectra. Effects of pulse imperfections are reduced by the alternation of the phases of the π pulses indicated in Figure 4b. Since the intensity of the signals at $\nu_1 = 0$ is not considered in our analysis of the DD/CSA spectra (see below), pulse imperfections do not affect the analysis significantly. A detailed discussion of the DD/CSA exchange technique, including examples of two-dimensional spectra of model compounds, is given in ref 10.

Purely absorptive CSA/CSA exchange spectra were acquired as interleaved, "hypercomplex" data sets, with the phase of the $\pi/2$ pulse at the end of t_1 alternating between x and y. Purely absorptive, symmetrized DD/CSA exchange spectra were obtained by discarding the imaginary part of the complex signal after Fourier transformation with respect to t_2 and phase correction and before Fourier transformation with respect to t_1. Final two-dimensional spectra were 256 × 256 points in size.

Two-dimensional NMR experiments were carried out using a Chemagnetics CMX-400 NMR spectrometer, operating at a ^{13}C NMR frequency of 100.47 MHz, and a home-built double-resonance, variable-temperature NMR probe. Sample weights were roughly 100 mg. In the CSA/CSA experiments, between 64 and 128 complex t_1 points were taken, with 96–512 scans per t_1 value and a recycle delay of 2–4 s (total acquisition time ~ 30–150 h). ^{13}C $\pi/2$ pulse lengths of 3.5 μs and proton decoupling fields of 50 kHz were used. In the DD/CSA experiments, 32 t_1 points were taken, with 64–1400 scans per t_1 value and a recycle delay of 2 s (total acquisition time ~ 1–24 h). ^{13}C $\pi/2$ pulse lengths of 4.0 μs and proton decoupling fields of 100 kHz were used.

The t_1 interferograms obtained in the DD/CSA experiments (consisting of 32 data points each) exhibited large, slowly-decaying zero-frequency components. To avoid truncation artifacts in the Fourier transforms with respect to t_1, we calculated a least-squares fit of points 17–32 to a single-exponential decay for each interferogram and used the resulting exponential functions to fill in points 33–256 (rather than simply zero-filling the interferograms to 256 points) before performing the Fourier transforms. As a result of this procedure, the two-dimensional spectra

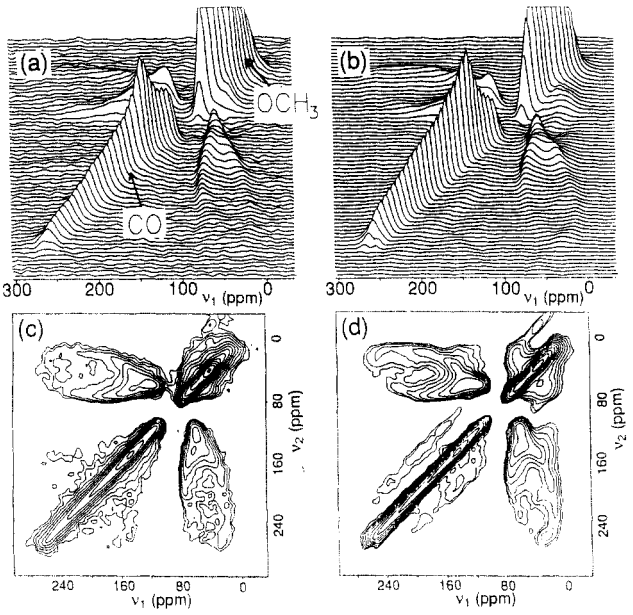

Figure 5. Two-dimensional ^{13}C NMR exchange spectra of selectively ^{13}C-enriched PMMA at 23 °C (a and c) and PMA at −100 °C (b and d), obtained with the rf pulse sequence in Figure 4a. $\tau = 2$ s. The same spectra are represented both as stack plots (a and b) and as contour plots (c and d). The diagonal features arising from the labeled carboxyl and methoxy sites are indicated. The off-diagonal intensity pattern contains the conformational information.

do appear to be free of truncation artifacts, but the intensities at $\nu_1 = 0$ are not reliable.

III. Conformations of Poly(methyl methacrylate) and Poly(methyl acrylate)

A. Experimental Two-Dimensional Spectra. Figure 5 shows two-dimensional ^{13}C CSA/CSA NMR exchange spectra of the isotopically enriched PMMA (parts a and c) and PMA (parts b and d), obtained with the exchange period $\tau = 2$ s. The PMMA spectrum was taken at room temperature. The PMA spectrum was taken at −100 °C. At these temperatures in the two cases, molecular reorientations are negligible on the time scale of τ. The spectra of the two samples are quite similar. In both cases, ridges of high intensity appear along the diagonal of the two-dimensional spectra at frequencies that correspond to the carboxyl and the aliphatic resonances. These ridges are due to nuclear magnetization that has the same frequency in both t_1 and t_2. In addition, there are "horseshoe-shaped" intensity ridges off of the diagonal at frequencies corresponding to the carboxyl resonance in one dimension and the methoxy resonance in the other dimension. These ridges are due to nuclear magnetization that changes its frequency during τ as a result of magnetization exchange between the carboxyl and methoxy sites *in a single monomer*. Maxima in the off-diagonal signal intensity occur near (ν_1, ν_2) equal to (120 ppm, 60 ppm) and (60 ppm, 120 ppm). The off-diagonal intensity pattern contains the desired information about the monomer conformation. The observed pattern clearly shows that the carboxyl and methoxy frequencies (anisotropic chemical shifts) are strongly correlated. In the absence of correlation (and in the fully-exchanged, or large τ, limit), all cross-sections through the off-diagonal intensity pattern, parallel to either the ν_1 or the ν_2 axis, would appear identical apart from the vertical scale. Of course, the strong correlations that we observe between the NMR frequencies of the exchanging carboxyl and methoxy carbons arise because the possible relative orientations of the two functional groups are constrained by the bonding geometry of the monomer. The fact that the off-diagonal intensity patterns in the PMMA and PMA spectra have nearly the same shape indicates that the monomer conformations are essentially the same in the two polymers.

There is some evidence for magnetization exchange among methoxy carbons *on different monomers* in the form of off-diagonal intensity at methoxy frequencies in both ν_1 and ν_2. This feature is stronger in the PMA spectrum than in the PMMA spectrum as expected given the higher level of isotopic enrichment in the PMA sample. The PMA spectrum also exhibits weak off-diagonal intensity ridges that run parallel to the diagonal. These are artifacts due to slight truncation of the data in the t_1 dimension.

We consider the low-intensity, off-diagonal features that appear to indicate magnetization exchange among carboxyl carbons in Figures 5c and 7 to be artifacts resulting from slight errors in phasing and baseline corrections of the two-dimensional spectra. However, we cannot rule out the possibility that these features are signatures of a small fraction (<5%) of monomers that execute large-amplitude reorientations on time scales less than 100 ms.

B. Comparison with Simulations in the Fully-Exchanged Limit. To extract conformational information from the two-dimensional NMR spectra, we compare them to simulated two-dimensional spectra for various possible conformations. In the fully-exchanged, or large τ, limit, the simulations are comparatively simple to carry out. Assuming an appropriate axis system fixed relative to the monomer (as in Figure 1), the carboxyl and methoxy carbons have chemical shifts

$$\delta^{(i)} = \delta_{11}{}^{(i)}(\hat{n}_{11}{}^{(i)}\cdot\hat{b})^2 + \delta_{22}{}^{(i)}(\hat{n}_{22}{}^{(i)}\cdot\hat{b})^2 + \delta_{22}{}^{(i)}(\hat{n}_{22}{}^{(i)}\cdot\hat{b})^2 \quad (1)$$

where $\{\delta_{\alpha\alpha}{}^{(i)}\}$ and $\{\hat{n}_{\alpha\alpha}{}^{(i)}\}$ are the principal values and principal axis directions of the CSA tensor for carbon i (i equals 1 for the carboxyl and 2 for the methoxy carbon) and $\hat{b}$ is the direction of the external magnetic field.[2] The CSA principal values are known from the one-dimensional ^{13}C powder pattern spectra. The principal axis directions depend on the orientation of the CSA tensor relative to the functional group itself (see below) and on the assumed conformation of the monomer. For a given conformation, we add together the contributions to the two-dimensional spectrum from a representative grid of external field directions (2.5×10^4 directions in the simulations shown below). For each field direction, we add one unit of intensity to each of the four positions $(\delta^{(1)},\delta^{(1)})$, $(\delta^{(1)},\delta^{(2)})$, $(\delta^{(2)},\delta^{(1)})$, and $(\delta^{(2)},\delta^{(2)})$ in the spectrum. This calculation of the intensities corresponds to the fully-exchanged limit because it implies that nuclear magnetization with frequency $\delta^{(1)}$ in t_1 is equally likely to have frequencies $\delta^{(1)}$ and $\delta^{(2)}$ in t_2, and vice versa. We then apply an empirically-based smoothing function to the simulated spectrum to approximate the line widths in the experimental spectra.

The CSA principal axis directions are known only approximately from studies of model compounds.[8,13,21-24] We therefore fixed $\hat{n}_{33}{}^{(1)}$ to be normal to the O=C–O plane (the yz plane in Figure 1a) and $\hat{n}_{33}{}^{(2)}$ to be parallel to the O–CH_3 bond, in agreement with model compound studies, but allowed the angle ζ_1 between $\hat{n}_{22}{}^{(1)}$ and the C=O bond (with positive values of ζ_1 representing rotations toward the C–O bond) and the angle ζ_2 between $\hat{n}_{22}{}^{(2)}$ and the direction normal to the C–O–CH_3 plane to vary. We set $\Theta_1 = 66°$ and $\Theta_2 = 125°$ (see Figure 1a), based on previous structural studies of methyl ester compounds.[25,26] Two-dimensional CSA/CSA exchange spectra were calculated for all combinations of values of the three variables ζ_1, ζ_2,

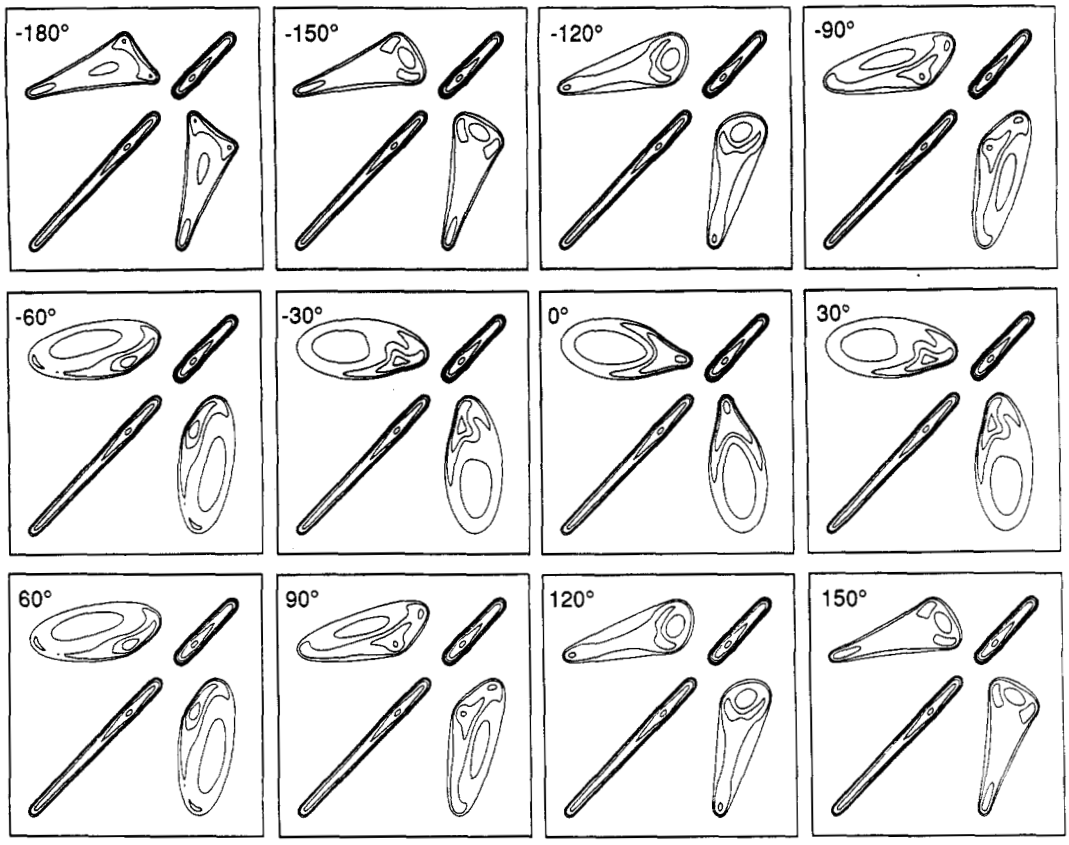

Figure 6. Simulated ^{13}C CSA/CSA NMR exchange spectra, appropriate for both PMMA and PMA in the fully-exchanged limit. The value of the dihedral angle χ_1 is indicated on each spectrum. All other parameters are fixed as described in the text.

and the dihedral angle χ_1, initially in 30° increments over the entire ranges of values and finally in 10° increments over restricted ranges, and were compared with the experimental spectra. *Qualitative agreement between the experimental and the simulated spectra occurs only when* $\zeta_1 = 10 \pm 10°$, $\zeta_2 = 0 \pm 10°$, *and* $\chi_1 = 0 \pm 10°$. *Thus, we determine that the methyl ester side groups in both PMMA and PMA have planar, trans conformations.* In addition, we determine the CSA tensor orientations, specifically that $\hat{n}_{22}^{(2)}$ is perpendicular to the C–O–CH_3 plane and $\hat{n}_{22}^{(1)}$ lies in the O=C–O plane at a 10° angle from the C=O bond. Examples of the simulated two-dimensional spectra are shown in Figure 6. In this series of spectra, ζ_1 and ζ_2 are kept constant at 10 and 0°, respectively, and χ_1 takes on the indicated values. The experimentally observed, horseshoe-shaped pattern of off-diagonal intensity only appears near $\chi_1 = 0°$. Only near $\chi_1 = 0°$ do the maxima in the off-diagonal intensity occur at the positions observed in the experimental spectra (see above). At other values of χ_1, off-diagonal intensity appears in regions of the $\nu_1\nu_2$ plane where there is no intensity in the experimental spectra and the shape of the off-diagonal intensity pattern does not agree with the experimental observations.

C. Comparison with Simulations in the Partially-Exchanged Limit. Additional insight into the experimental two-dimensional spectra of PMMA and PMA comes from a comparison between the experimental and calculated dependences of the spectra on τ, shown in Figure 7. In both the experiments and the simulations, the off-diagonal intensity pattern does not grow in uniformly with increasing τ. Rather, disconnected regions of high intensity appear first and then gradually meld to produce the large-τ limit. This behavior is a result of the complicated dependence of the rate of nuclear magnetization exchange on the monomer orientation. Taking into

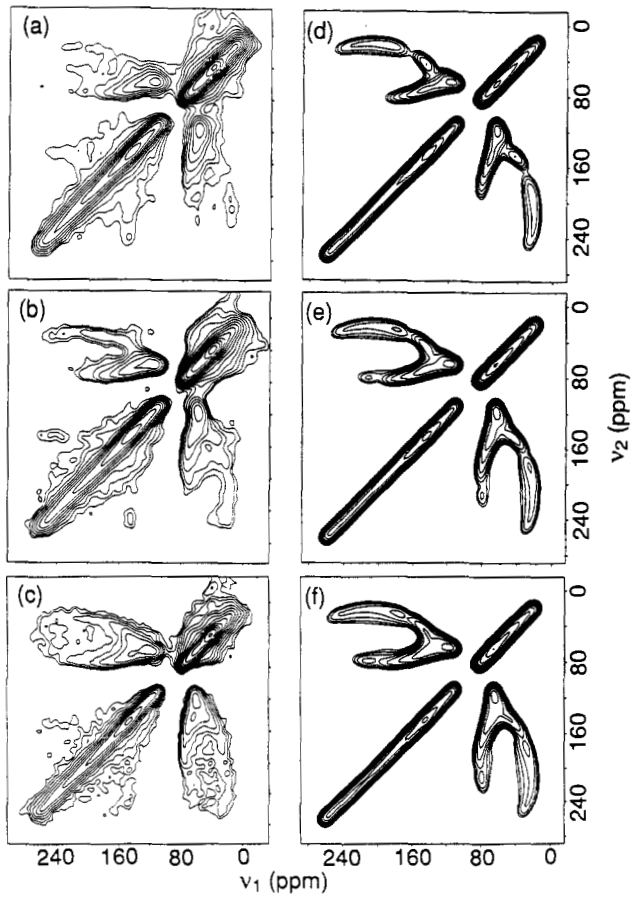

Figure 7. Experimental (a, b, and c) and simulated (d, e, and f) dependences of the ^{13}C CSA/CSA NMR exchange spectrum of selectively ^{13}C-enriched PMMA on the exchange period τ. τ has the values 0.1 s in (a) and (d), 0.5 s in (b) and (e), and 2 s in (c) and (f).

account this dependence, as described in the following discussion, leads to a more quantitative agreement between the experiments and the simulations.

The simulations in Figure 7 are carried out as in the fully-exchanged limit except for the assignment of intensities to the four positions $(\delta^{(1)},\delta^{(1)})$, $(\delta^{(1)},\delta^{(2)})$, $(\delta^{(2)},\delta^{(1)})$, and $(\delta^{(2)},\delta^{(2)})$ in the two-dimensional spectrum. These intensities are given by $^1/_2(1 + e^{-k\tau})$, $^1/_2(1 - e^{-k\tau})$, $^1/_2(1 - e^{-k\tau})$, and $^1/_2(1 + e^{-k\tau})$, respectively, where k is the rate of magnetization exchange. A simple theory of magnetization exchange between ^{13}C nuclei in organic solids[3] shows that

$$k = d^2 \int_0^\infty dt\ \mathrm{Re}[F_1(t)\ F_2^*(t)] \tag{2}$$

where d is the magnetic dipole–dipole coupling constant for the two nuclei (in rad/s) and $F_1(t)$ and $F_2(t)$ are the NMR free-induction-decay (fid) signals of the two nuclei, with $F_i(0) = 1$. d is given by

$$d = \frac{\gamma^2 \hbar}{r^3} \frac{1 - 3\cos^2\Theta}{2} \tag{3}$$

where γ is the nuclear gyromagnetic ratio, r is the internuclear distance, and Θ is the angle between the internuclear vector and the external field. In the present case, $r \approx 2.33$ Å.

The functions $F_i(t)$ are determined primarily by the carbon CSA tensors and by the *proton–carbon* dipole–dipole couplings, since magnetization exchange takes place in the absence of proton decoupling in our experiments. To be precise, the $F_i(t)$ are undecoupled fids of carbon nuclei on monomers with specific *orientations* relative to the external field. These are not experimentally accessible. However, reasonable approximations to these fids can be determined from two-dimensional separated-local-field (SLF) NMR spectra,[27,28] which give the undecoupled signals of carbon nuclei on monomers with specific *chemical shifts*. Such an SLF spectrum of PMA, obtained simply by using the pulse sequence in Figure 4a without decoupling during the t_1 period and with $\tau = 1$ ms, is shown in Figure 8a. One-dimensional slices through the two-dimensional spectrum parallel to the ν_1 axis show that the undecoupled spectrum of the carboxyl carbons is a singlet (Figure 8b), while that of the methoxy carbons is a quartet (Fgure 8c) with intensity ratios 1:3:3:1 due to the carbon–proton couplings within the (rapidly rotating) methyl group. The fact that the largest carbon–proton coupling occurs at the upfield edge of the methoxy CSA powder pattern supports our earlier assumption that $\hat{n}_{33}^{(2)}$ is parallel to the O–CH_3 bond. For both the carboxyl and the methoxy carbons, couplings to more distant protons produce a broadening of the lines that we take to be Gaussian, with a full-width at half-maximum of 4 kHz. We therefore assume the following forms for $F_1(t)$ and $F_2(t)$:

$$F_1(t) = e^{i\gamma B_0 \delta^{(1)} t} e^{-gt^2} \tag{4a}$$

$$F_2(t) = \frac{1}{4} e^{i\gamma B_0 \delta^{(2)} t} (\cos 3\Delta t + 3\cos \Delta t) e^{-gt^2} \tag{4b}$$

B_0 is the external field strength, $\delta^{(1)}$ and $\delta^{(2)}$ are the chemical shifts (which depend on the field direction as in eq 1), $g = 5.7 \times 10^5\ s^{-2}$, and Δ is the proton–carbon splitting for the methoxy carbon, given by $\Delta = {}^1/_2(1 - 3\cos^2\alpha) \times 4.7 \times 10^4\ s^{-1}$ where α is the angle between the O–CH_3 bond and the external field. The simulations in Figure 8 also assume the values $\zeta_1 = 10°$, $\zeta_2 = 0°$, and $\chi_1 = 0°$ derived above.

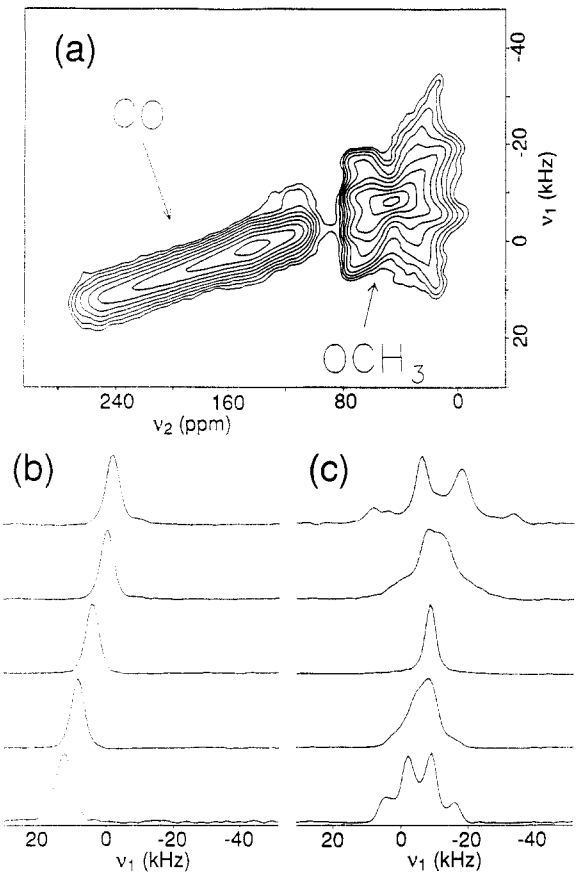

Figure 8. (a) Two-dimensional separated-local-field (SLF) NMR spectrum of selectively ^{13}C-enriched PMA, obtained at −100 °C. Frequencies in the ν_2 dimension are determined by the ^{13}C chemical shifts. Frequencies in the ν_1 dimension are determined both by the ^{13}C chemical shifts and by carbon–proton magnetic dipole–dipole couplings. (b) Cross-sections of the SLF spectrum parallel to the ν_1 axis in the carboxyl region. From top to bottom, the ν_2 values are 112.1, 127.7, 169.2, 210.6, and 252.1 ppm. (c) Cross-sections of the SLF spectrum parallel to the ν_1 axis in the methoxy region. From top to bottom, the ν_2 values are 13.6, 29.2, 44.8, 60.3, and 75.9 ppm. These line shapes are used to guide the simulations in Figure 7.

IV. Conformation of Poly(ethyl methacrylate)

A. Experimental Two-Dimensional Spectra. Two-dimensional DD/CSA exchange experiments were carried out to probe the monomer conformation in PEMA, using the pulse sequence in Figure 4b. We encountered several experimental difficulties that made the results of these experiments less definitive than the results for PMMA and PMA described above. First, we found that molecular motion interfered with the detection of carbon–carbon dipole–dipole couplings within the labeled ethoxy groups at room temperature. The Carr–Purcell train in the t_1 dimension of the pulse sequence did not produce the desired dipolar powder pattern (Pake pattern) spectrum for the ethoxy carbons.[10,20] We were therefore forced to carry out the experiments at −100 °C, where molecular motion no longer affected the results. Unfortunately, the spin–lattice relaxation time (T_1) of the methyl carbon in the ester group decreases with decreasing temperature, reaching roughly 0.25 s at −100 °C. Since the exchange period τ cannot greatly exceed T_1 in these experiments, we were limited to values of $\tau \leq 0.5$ s. Even at $\tau = 0.5$ s, the magnetization exchange within a monomer is incom-

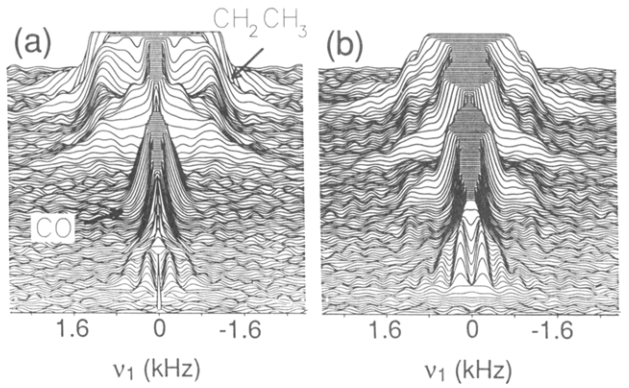

Figure 9. Two-dimensional ^{13}C DD/CSA NMR exchange spectra of selectively ^{13}C-enriched PEMA, obtained at −100 °C with τ = 1 ms (a) and τ = 0.5 s (b). The spectra were obtained with the rf pulse sequence in Figure 4b. Features arising from the labeled ethoxy and carboxyl sites are indicated in (a). The additional intensity in the carboxyl region away from $\nu_1 = 0$ in (b) contains the conformational information.

plete, there is substantial loss of signal intensity due to spin–lattice relaxation during τ, and the dipolar line shapes are somewhat distorted by the anisotropy of the relaxation rate. Nonetheless, the results of these experiments do provide information, albeit incomplete, about the monomer conformation in this polymer. In addition, the results demonstrate the potential of this approach for structural studies in other systems.

Two-dimensional ^{13}C DD/CSA NMR exchange spectra of the PEMA sample are shown in Figure 9. At τ = 1 ms (Figure 9a), there is essentially no exchange of nuclear magnetization between the carboxyl and ethoxy carbons. The labeled ethoxy carbons give rise to a mound of intensity whose width in the ν_1 dimension is due primarily to the strong carbon–carbon dipole–dipole couplings within the ethoxy group and whose width in the ν_2 dimension is due to both the dipole–dipole couplings and the CSA. The labeled carboxyl carbons give rise to a ridge of intensity near $\nu_1 = 0$ whose width in the ν_2 dimension is due to the CSA. The width of this ridge in ν_1 in Figure 9a is due to the comparatively weak couplings between the carboxyl carbon and the ethoxy carbons and to imperfections in the Carr–Purcell train. At τ = 0.5 s (Figure 9b), the dipolar splittings of the ethoxy carbons in ν_1 are transferred in part to the carboxyl carbon ridge. It is the intensity pattern of these transferred dipolar splittings that contains the desired conformational information.

B. Comparison with Simulations. To interpret the DD/CSA exchange spectra of PEMA in terms of the monomer conformation, we carried out simulations of the important region of the DD/CSA spectrum (i.e., the carboxyl ridge) for various possible conformations in the fully-exchanged limit. The computational method for these simulations is quite similar to the method described in section III.B. The principal difference is that the NMR frequencies in the two dimensions of the spectrum are not the same in this case. For a given conformation and a given external field direction relative to the monomer, the frequency in ν_2 is the carboxyl chemical shift $\delta^{(1)}$. The possible frequencies in ν_1 are 0, $+d_{ee}$, and $-d_{ee}$, where d_{ee} is the carbon–carbon dipolar splitting of the ethoxy carbons given by

$$d_{ee} = \frac{3\gamma^2\hbar}{4r_{ee}^3}[3(\hat{r}_{ee}\cdot\hat{b})^2 - 1] \qquad (5)$$

r_{ee} is the length and $\hat{r}_{ee}$ is the direction of the ethoxy carbon–carbon bond. For the fully-exchanged limit, we assign intensities 1, 2, and 1 to positions $(\delta^{(1)},-d_{ee})$, $(\delta^{(1)},0)$, and $(\delta^{(1)},d_{ee})$ in the simulated spectrum. We assume the same CSA tensor orientation for the carboxyl carbon in PEMA as derived for PMMA and PMA in section III. In the notation of Figure 1b, we take $\Theta_3 = 125°$, $\Theta_2 = 114°$, and $\Theta_1 = 70.5°$. The conformation is then described by the two dihedral angles χ_1 and χ_2. Based on the results in section III and on previous structural studies, we fix $\chi_1 = 0°$.

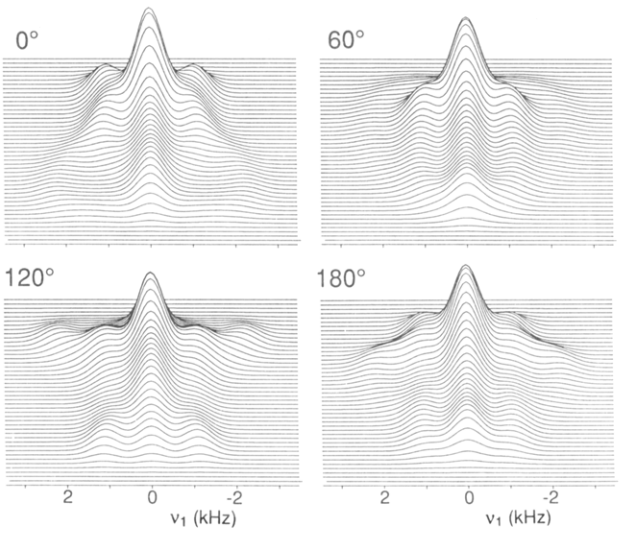

Figure 10. Simulated ^{13}C DD/CSA NMR exchange spectra, appropriate for PEMA in the fully-exchanged limit. Only the carboxyl region is shown. The value of the dihedral angle χ_2 is indicated on each spectrum. All other parameters are fixed as described in the text.

Figure 10 shows simulated DD/CSA spectra for several values of χ_2. The spectra are clearly sensitive to the assumed conformation. The most striking differences among the spectra are in the shapes of the low-intensity features associated with the largest dipolar splittings in ν_1. However, for the reasons discussed above, these features are not apparent in the experimental spectra. Figure 11 compares the carboxyl region of the experimental spectra with the simulations, with both represented as contour plots. Only the higher contours of the simulations are displayed to facilitate the comparison. In the contour plot representation, the most significant difference between the experimental spectra at τ = 1 ms (Figure 11a) and τ = 0.5 s (Figure 11b) is the higher intensity at τ = 0.5 s in the band between ν_2 = 120 ppm and ν_2 = 155 ppm. This band is delineated by dotted lines in all spectra in Figure 11. The simulated spectra have their highest intensity within this band only for χ_2 near 0° (Figure 11c) or 180° (Figure 11i). The agreeement in the widths in the ν_1 dimension of the high-intensity features of the experimental and simulated spectra appears somewhat better near $\chi_2 = 0°$. We therefore conclude that the monomers in PEMA are most likely to have a planar, all-trans conformation.

V. Discussion and Conclusions

A. Poly(methyl methacrylate) and Poly(methyl acrylate). The results for PMMA and PMA are quite conclusive, showing that the methyl ester side group has a well-defined, planar conformation in these amorphous solids. This is in spite of the fact that steric effects alone do not force a planar conformation, as can be seen from space-filling models of the two polymers. The absence of the pendant methyl group in PMA would appear to make

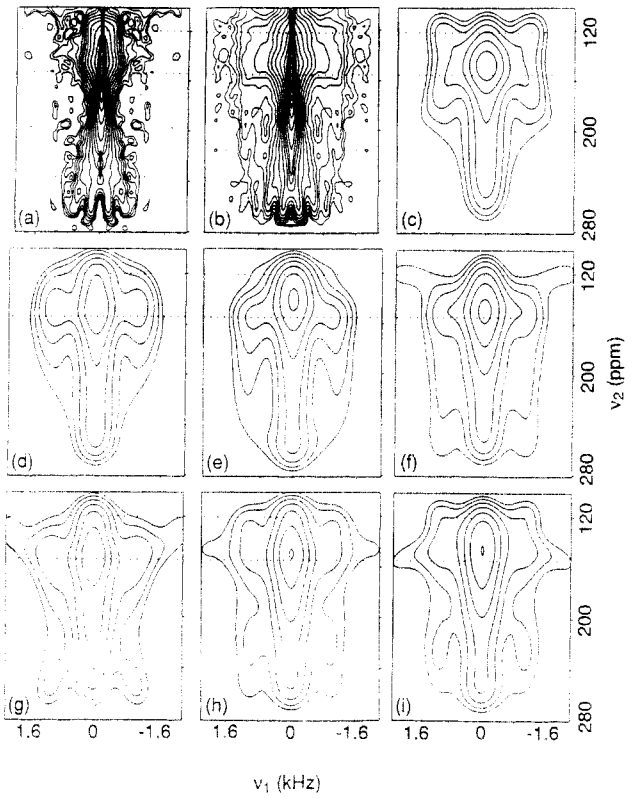

Figure 11. Experimental (a and b) and simulated (c–i) ^{13}C DD/CSA NMR exchange spectra of PEMA, represented as contour plots. τ = 1 ms in (a). τ = 0.5 s in (b). χ_2 has the values 0, 30, 60, 90, 120, 150, and 180° in (c–i), respectively. All other parameters in the simulations are fixed as described in the text.

steric effects even less important, yet the conformation of the PMA monomer is no less well-defined than that of the PMMA monomer as evidenced by the sharpness of the off-diagonal intensity patterns in the CSA/CSA exchange spectra in Figure 5. We have also looked for possible effects of thermal history on the two-dimensional CSA/CSA exchange spectrum of PMMA, comparing the results shown in Figure 5 with results obtained after both rapid and slow cooling of the sample from temperatures above T_g. We find no effects. All of these results are in line with the generally accepted understanding of the conformations of methyl ester groups, according to which the planar conformation is stabilized by delocalization of electron pairs between the ether oxygen and the carbonyl group within the ester group.[29] The $\chi_1 = 0°$ form is also generally more stable than the $\chi_1 = 180°$ form. Our results show that the intramolecular electronic effects which stabilize the planar conformation are dominant even in the noncrystalline solid state.

The agreement between the experimentally observed and calculated dependences of the two-dimensional spectra on τ, shown in Figure 7, provides support for the expression for k given in eq 2 and for the idea that it is possible to understand the rates of ^{13}C magnetization exchange in complex organic solids quantitatively.[3-5] A quantitative understanding of these rates allows additional structural information to be derived from two-dimensional NMR exchange spectroscopy.[3,9]

B. Poly(ethyl methacrylate). The conformations of ethyl ester groups are considerably more variable. Although the planar ($\chi_1 = 0°$, $\chi_2 = 0°$) conformation is frequently found in crystalline compounds, many examples of crystalline compounds with χ_2 substantially different from 0° exist.[30] In the gas phase,[31] the difference in energy between the $\chi_2 = 0°$ and the $\chi_2 \approx 120°$ (gauche) conformers of ethyl formate is only 190 cal/mol. These two conformers are separated by an energy barrier of only 1100 cal/mol. The $\chi_2 = 180°$ conformer is higher in energy by 5000 cal/mol. The preferred monomer conformation in PEMA is therefore not known *a priori*. The two-dimensional DD/CSA spectra suggest that the planar conformation is the predominant one, but we cannot rule out the possibility that other conformations are present in appreciable numbers. In fact, our observation of significant molecular dynamics well below T_g supports this possibility.

Higher quality data would allow us to determine the conformation, or conformational distribution, with greater certainty. Unfortunately, the NMR relaxation properties of the ethyl ester side group in PEMA make it difficult for us to improve the data, as explained above. One possible approach may be to carry out the DD/CSA exchange experiments at lower magnetic field strengths where the rates of magnetization exchange may be accelerated due to increased spectral overlap between the carboxyl and ethoxy resonances.

With the exception of certain methyl carbons, ^{13}C nuclei in solids generally have relaxation times that greatly exceed several seconds near room temperature. Since our experiments and simulations show that τ values of several seconds are sufficient for the acquisition of a useful two-dimensional exchange spectrum, we do not expect the NMR relaxation properties to preclude the use of exchange spectroscopy as a probe of molecular conformations in most systems.

C. Extensions. Our results show that two-dimensional ^{13}C NMR exchange spectroscopy is capable of providing essentially "crystallographic" information about molecular conformations in noncrystalline solids. The method is applicable to any system that can be specifically labeled appropriately. Although the fact that the labeled sites have resolved powder pattern line shapes in the one-dimensional ^{13}C NMR spectrum simplifies the interpretation of the two-dimensional spectra, this is not a requirement. For example, our earlier work on molecular orientational ordering in solid methanol[8] showed that structural information could be obtained from two-dimensional exchange experiments on singly-labeled compounds, where the exchanging sites necessarily have unresolved powder pattern line shapes in the one-dimensional spectrum. The method should therefore have widespread applications in structural studies of synthetic polymers, biopolymers, and other complex organic systems. For example, it should be possible to determine the conformations of plasticizers added to synthetic polymers, substrates bound to biological or synthetic enzymes, and molecular dopants in glasses.

The same techniques may be applied to the study of intermolecular interactions. If complementary sites are isotopically labeled on two different components of an intermolecular complex, supramolecular assembly, or blend, the two-dimensional spectrum resulting from exchange of magnetization between these sites will contain information about the relative orientations of the two components. Such information should contribute to the understanding of the structure of the complex, assembly, or blend. This approach should be useful in studies of intermolecular interactions in compatible polymer blends, interactions between polypeptides in biological membrane channels, solvent–solute interactions in frozen solutions, and interactions in many other systems. We are currently pursuing work along these lines.

Some of these proposed applications of NMR exchange spectroscopy may require modifications of the experi-

mental techniques. In the experiments described above, natural-abundance ^{13}C NMR signals do not interfere with the analysis of the spectra because of the relatively high concentration of the labeled sites (i.e., most of the signal comes from the labeled sites rather than the natural-abundance sites). The signals from the labeled sites are also sufficiently strong that magic-angle spinning (MAS) is not required to enhance the sensitivity. This will generally be the case in experiments on small molecules, synthetic polymers, or any other system in which the structural unit under investigation does not comprise only a small fraction of the total sample. However, in applications to complex biochemical systems, where the labeled sites of interest may be greatly diluted in unlabeled material, it may prove necessary to employ MAS to enhance the sensitivity and double-quantum filtering[32-34] or difference spectroscopy to suppress natural-abundance signals. MAS versions of the techniques described above that depend on the analysis of two-dimensional spinning sideband patterns are readily envisioned. Switching of the spinning angle[34] may be required to accelerate the exchange of nuclear magnetization during τ.

Finally, it is worth pointing out that a number of new NMR techniques for studying molecular conformations, based on measurements of *internuclear distances*, have been developed in recent years.[35-38] The methods used in this paper differ in that their primary emphasis is on the determination of the *relative orientations* of chemical bonds and functional groups rather than the distances between nuclei. The two approaches to structural studies are largely complementary, as there are cases in which a structural property is best defined in terms of internuclear distances and cases (such as those treated in this paper) in which a structural property is best defined in terms of angles that characterize the relative orientations of bonds and functional groups.

References and Notes

(1) Jeener, J.; Meier, B. H.; Bachmann, P.; Ernst, R. R. *J. Chem. Phys.* **1979**, *71*, 4546.
(2) Mehring, M. *Principles of High Resolution NMR in Solids*, 2nd ed.; Springer-Verlag: New York, 1983.
(3) Tycko, R.; Dabbagh, G. *Isr. J. Chem.* **1992**, *32*, 179.
(4) Suter, D.; Ernst, R. R. *Phys. Rev. B* **1985**, *32*, 5608.
(5) Henrichs, P. M.; Linder, M. *J. Chem. Phys.* **1986**, *85*, 7077.
(6) Schmidt, C.; Blümich, B.; Spiess, H. W. *J. Magn. Reson.* **1988**, *79*, 269.
(7) Blümich, B.; Spiess, H. W. *Angew. Chem., Int. Ed. Engl.* **1988**, *27*, 1655.
(8) Tycko, R.; Dabbagh, G. *J. Am. Chem. Soc.* **1991**, *113*, 3592.
(9) Tycko, R.; Dabbagh, G. *Mater. Res. Soc. Symp. Proc.* **1991**, *215*, 125.
(10) Weliky, D. P.; Dabbagh, G.; Tycko, R. *J. Magn. Reson.* **1993**, *A104*, 10.
(11) Edzes, H. T.; Bernards, J. P. C. *J. Am. Chem. Soc.* **1984**, *106*, 1515.
(12) Henrichs, P. M.; Linder, M. *J. Magn. Reson.* **1984**, *58*, 458.
(13) Meier, B. H.; Ernst, R. R. *J. Am. Chem. Soc.*, in press.
(14) Meier, B. H.; Ernst, R. R. *J. Am. Chem. Soc.* **1979**, *101*, 6441.
(15) Macura, S.; Ernst, R. R. *Mol. Phys.* **1980**, *41*, 95.
(16) Kumar, A.; Ernst, R. R.; Wüthrich, K. *Biochem. Biophys. Res. Commun.* **1980**, *95*, 1.
(17) Bovey, F. A. *Nuclear Magnetic Resonance Spectroscopy*, 2nd ed.; Academic Press: New York, 1988.
(18) Pham, Q. T.; Petiaud, R.; Llauro, M. F.; Waton, H. *Proton and Carbon NMR Spectra of Polymers*; John Wiley and Sons: New York, 1984.
(19) Edzes, H. T. *Polymer* **1983**, *24*, 1425.
(20) Engelsberg, M.; Yannoni, C. S. *J. Magn. Reson.* **1990**, *88*, 393.
(21) Chang, J. J.; Griffin, R. G.; Pines, A. *J. Chem. Phys.* **1975**, *62*, 4923.
(22) Griffin, R. G.; Ruben, D. J. *J. Chem. Phys.* **1975**, *63*, 1272.
(23) Ganapathy, S.; Chacko, V. P.; Bryant, R. G. *J. Chem. Phys.* **1984**, *81*, 661.
(24) Cornell, B. A. *J. Chem. Phys.* **1986**, *85*, 4199.
(25) Kroon, J.; Kanters, J. A. *Acta Crystallogr.* **1973**, *B29*, 1278.
(26) Curl, R. F., Jr. *J. Chem. Phys.* **1959**, *30*, 1529.
(27) Hester, R. K.; Ackerman, J. C.; Neff, B. L.; Waugh, J. S. *Phys. Rev. Lett.* **1976**, *36*, 1081.
(28) Linder, M.; Hohener, A.; Ernst, R. R. *J. Chem. Phys.* **1980**, *73*, 4959.
(29) Deslongchamps, P. *Stereoelectronic Effects in Organic Chemistry*; Pergamon Press: New York, 1983.
(30) For example: (a) Briant, C. E.; Jones, D. W. *Acta Crystallogr.* **1990**, *C46*, 2205. (b) Robert, P. F.; Jeannin, Y.; Vincent, M.; Laubie, M. *Acta Crystallogr.* **1984**, *C40*, 1219. (c) van Koningsveld, H.; Jansen, J. C.; Jongejan, J. A.; Jzn, J. F.; Duine, J. A. *Acta Crystallogr.* **1985**, *C41*, 89. (d) Watson, W. H.; Nagl, A.; Marchand, A. P.; Vidyasagar, V. *Acta Crystallogr.* **1990**, *C46*, 152.
(31) Riveros, J. M.; Wilson, E. B. *J. Chem. Phys.* **1967**, *46*, 4605.
(32) Tycko, R.; Dabbagh, G. *J. Am. Chem. Soc.* **1991**, *113*, 9444.
(33) Tycko, R.; Smith, S. O. *J. Chem. Phys.* **1993**, *98*, 932.
(34) Tycko, R. *J. Am. Chem. Soc.* **1994**, *116*, 2217.
(35) Tycko, R.; Dabbagh, G. *Chem. Phys. Lett.* **1990**, *173*, 461.
(36) Levitt, M. H.; Raleigh, D. P.; Creuzet, F.; Griffin, R. G. *J. Chem. Phys.* **1990**, *92*, 6347.
(37) Gullion, T.; Vega, S. *Chem. Phys. Lett.* **1992**, *194*, 423.
(38) Gullion, T.; Schaefer, J. *J. Magn. Reson.* **1989**, *81*, 196.